Superconductivity in noncentrosymmetric NbReSi investigated by muon spin rotation and relaxation

Sajilesh K. P.,[1] K. Motla,[1] P. K. Meena,[1] A. Kataria,[1] C. Patra,[1] Somesh K.,[1] A. D. Hillier,[2] and R. P. Singh[1,*]

[1]*Department of Physics, Indian Institute of Science Education and Research Bhopal, Bhopal 462066, India*

[2]*ISIS Facility, STFC Rutherford Appleton Laboratory, Harwell Science and Innovation Campus, Oxfordshire OX11 0QX, United Kingdom*

(Received 14 November 2021; revised 3 February 2022; accepted 21 March 2022; published 31 March 2022)

Noncentrosymmetric materials are a promising paradigm to explore unconventional superconductivity. In particular, several Re-containing noncentrosymmetric materials have attracted considerable attention due to a superconducting state with broken time-reversal symmetry. A comprehensive study on the superconducting ground state of NbReSi was performed using magnetization, resistivity, and muon spin rotation/relaxation measurements. Zero-field muon spectroscopy results showed the absence of spontaneous magnetic field below the superconducting transition temperature, $T_c = 6.29(3)$ K, indicating the preserved time-reversal symmetry. Transverse field muon spin rotation measurements confirms an s-wave nature of the sample with $\Delta(0)/k_BT_c = 1.73(2)$.

DOI: 10.1103/PhysRevB.105.094523

I. INTRODUCTION

Despite decade-long research on understanding the pairing mechanism in unconventional superconductors, the experimental evidence of exotic superconducting properties in various systems is still under debate among condensed matter physicists [1,2]. The field has observed a surge in research interest since the discovery of coexisting superconducting and antiferromagnetic phases in heavy-fermion noncentrosymmetric compound $CePt_3Si$, along with the unusual superconducting nature [3]. Recent evidence of protected topological surface states in superconductors has renewed interest in noncentrosymmetric (NCS) systems due to the possibility of hosting Majorana fermions, an emergent collective excitation of electrons [4,5]. An intrinsic antisymmetric spin-orbit coupling (ASOC) in these systems is expected to perturb the energy of electrons at the Fermi level and lead to the nontrivial pairing of electrons [6–8]. Such a scenario is expected to host unconventional features like a high upper critical field exceeding the Pauli limiting field, anisotropic/multiple superconducting gaps, magnetoelectric effects and topologically protected surface states [3,9–18].

One of the most intriguing properties of NCS superconductors is a spontaneous field in the superconducting ground state and hence the broken time-reversal symmetry (TRS). Among NCS systems, the materials displaying a broken TRS include $LaNiC_2$ [12], La_7X_3 (X = Ir, Rh, Ni) [19–21], Re_6X (X = Zr, Hf, Ti) [22–24], and CaPtAs [25]. An interesting case study is of NCS Re_6X, where members from this family have shown a spontaneous field with almost the same strength, irrespective of the X element. This result undermines the proposed effects of ASOC on the superconducting ground state. Moreover, the spontaneous field in the superconducting ground state of elemental Re powder with centrosymmetric structure has further added curiosity [26]. A very recent report on $Re_{1-x}Mo_x$ alloys has shown TRS breaking for $x = 0.12$, which crystallizes in the centrosymmetric structure. In contrast, it showed a preserved time-reversal state for all other compositions, including the noncentrosymmetric α-Mn structure [27]. Also, Re_3W [28] and Re_3Ta [29] both crystallizing in the α-Mn structure has also failed to show any spontaneous field in the superconducting state. Another binary compound, $ReBe_{22}$, which crystallizes in centrosymmetric structure, has shown TRS is preserved [30]. Although there are claims of the role played by elemental Re concentration, it is not yet verified. Hitherto, most of the Re-based systems microscopically studied are Re rich in concentration, except the $ReBe_{22}$ and $Re_{1-x}Mo_x$ ($x = 0.6$) superconductors. To further understand the role of structure and Re concentration, it is important to look for more Re-based superconductors with different Re concentrations, particularly having noncentrosymmetric crystal structures.

In this paper, we have investigated the nature of the superconducting ground state in NbReSi, containing an atomic ratio of 33% elemental Re. Superconductivity in this material was reported in 1985 [31]. NbReSi crystallizes in a noncentrosymmetric orthorhombic FeSiTi-type structure with a superconducting transition at 6.29(3) K. This structure is a superstructure modification of hexagonal ZrNiAl-type structure and shows a higher superconducting transition temperature. The high T_c in the hexagonal family is attributed to strong electron-phonon coupling strength, indicating the influence of structure on the superconducting properties of ternary equiatomic materials [32]. Here we have used the muon spin rotation/relaxation technique (μSR) to study the superconducting ground state of orthorhombic NbReSi. μSR in the longitudinal geometry without any externally applied field is an excellent tool to detect any spontaneous magnetic field arising below the superconducting transition, while μSR in

*rpsingh@iiserb.ac.in

transverse geometry with a small applied field can determine the temperature dependence of magnetic field distribution in the vortex state, giving information about the superconducting gap structure.

II. EXPERIMENTAL METHODS

A polycrystalline sample of NbReSi was prepared by arc melting stoichiometric amounts of the constituent elements on a water-cooled copper hearth under argon gas atmosphere. The samples were flipped and remelted several times and annealed for one week at 800°C in sealed quartz ampules under vacuum to ensure homogeneity. The sample characterization was done using x-ray powder diffraction on a PANalytical diffractometer using Cu K_α radiation ($\lambda = 1.54056$ Å). Both dc and ac magnetic susceptibility measurements were performed using a Quantum Design superconducting quantum interference device (QD-MPMS3). Magnetic measurements were taken in both zero field cooled warming (ZFCW) and field cooling (FCC) mode. The electrical property measurements were performed on a Quantum Design physical property measurement system. The μSR measurements were carried out using the MuSR spectrometer at the ISIS Neutron and Muon Facility in STFC Rutherford Appleton Laboratory, United Kingdom. The powdered sample of NbReSi was mounted on a high-purity-silver plate using diluted GE varnish. The μSR measurements were performed in the longitudinal and transverse-field geometries. During measurement, spin-polarized muons were implanted into the sample. In the longitudinal configuration, the positrons were detected either in forward or backward positions along the axis of the muon beam. The asymmetry is calculated using the equation

$$G_Z(t) = \frac{N_B - \alpha N_F}{N_B + \alpha N_F}, \quad (1)$$

where N_F and N_B are the number of counts at the detectors in the forward and backward positions, and α is determined from calibration measurements taken with a small applied transverse magnetic field. In this configuration, measurements were made in zero field where the contribution from the stray fields at the sample position due to neighboring instruments and the earth's magnetic field is canceled to within $\sim$1.0 μT by using three sets of orthogonal coils. In the transverse configuration, a field was applied perpendicular to the direction of the muon beam, and the detectors were grouped into two orthogonal pairs. A full description of the μSR technique may be found in Ref. [33].

III. RESULTS AND DISCUSSION

A. Crystallography

X-ray diffraction data collected at ambient pressure and temperature is shown in Fig. 1. Reitveld refinement of the data done using FULLPROF [34] software shows no impurity phase is present in sample. NbReSi adopts the orthorhombic FeSiTi-type structure which has the noncentrosymmetric space group, *Ima*2. The crystallographic parameters obtained are $a = 6.925(5)$ Å, $b = 11.671(2)$ Å, $c = 6.693(8)$ Å, in good agreement with reported data [31].

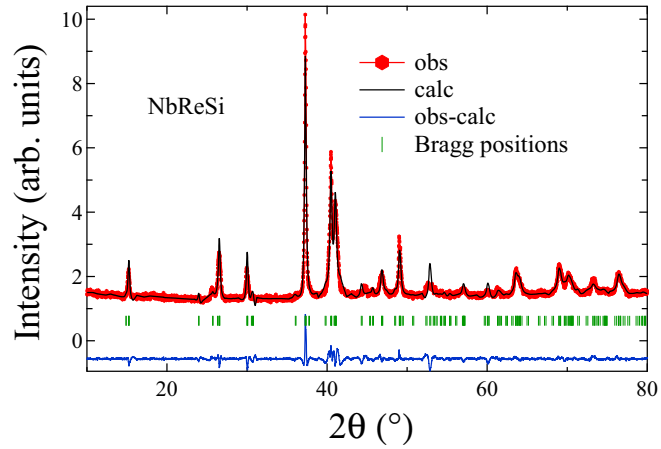

FIG. 1. The powder x-ray diffraction pattern collected at ambient temperature and pressure. The red markers show the observed pattern and the solid black line is the Rietveld refinement to the observed pattern. The blue lines indicate the difference between the observed and calculated peaks, whereas the green markers show the Bragg position.

B. Resistivity

Figure 2 shows the temperature dependence of the resistivity. Temperatures greater than 7 K show a small increase with temperature up to 300 K. However, below 10 K, a sudden drop in resistivity around 6.46(7) K marks the onset of superconductivity in NbReSi. Zero resistivity was observed at 6.14 K, which gives a transition width of $\Delta T = 0.32$ K. The metallic nature of the sample can be inferred from the positive slope shown above T_c ($\rho_{300\,K}/\rho_{10\,K} = 1.12$). The resistivity data above superconducting transition can be described by the Bloch-Gruneisen (BG) model. It takes into account the resistivity arising due to electrons scattering from longitudinal acoustic phonon [35]. According to this model, resistivity can

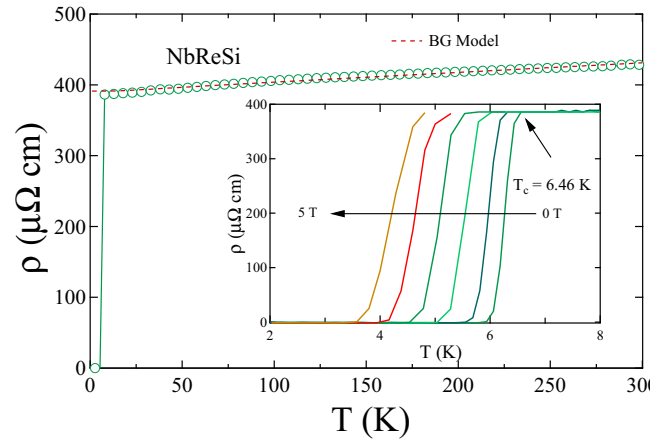

FIG. 2. Resistivity data taken at zero field showing a metallic nature of NbReSi. The inset shows the superconducting nature of the sample at zero applied field and different applied fields. The superconducting transition at zero field is at $T_c = 6.46(7)$ K. The normal state resistivity data in the range 20 K to 300 K is well described by the Bloch-Gruneisen (BG) model and is shown by a dotted red line.

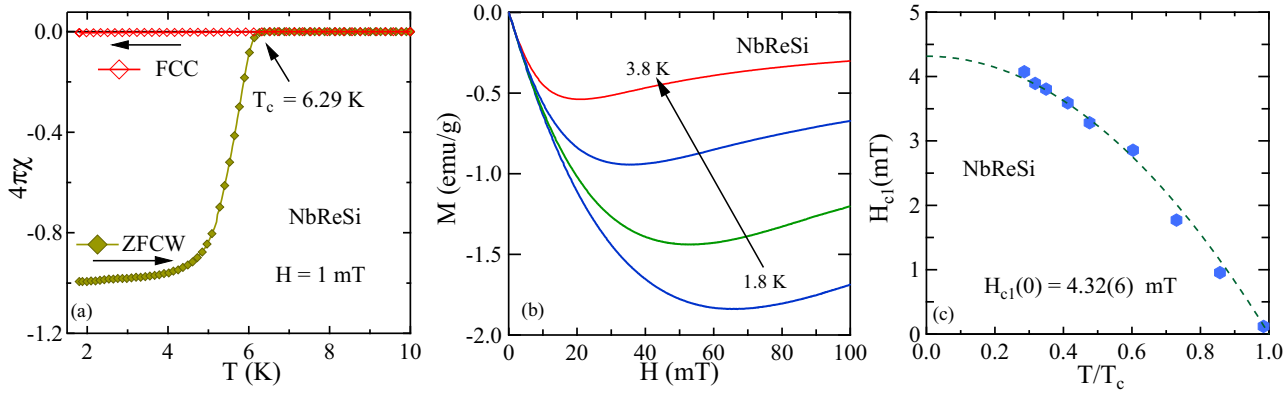

FIG. 3. (a) dc magnetization data were taken at an applied field of 1 mT, showing a superconducting transition at 6.29(3) K. (b) Low field magnetization curves taken at different temperatures (c) Lower critical field, H_{c1} versus normalized temperature for NbReSi. The dotted line showing fit to the data using GL equation gives $H_{c1}(0) = 4.32(6)$ mT

be defined as

$$\rho(T) = \rho_0 + \rho_{\mathrm{BG}}(T), \tag{2}$$

where $\rho_{\mathrm{BG}}(T)$ is defined as

$$\rho_{\mathrm{BG}}(T) = r\left(\frac{T}{\theta_D}\right)^5 \int_0^{\Theta_D/T} \frac{x^5}{(e^x - 1)(1 - e^{-x})} dx. \tag{3}$$

Here, θ_D is the Debye temperature, ρ_0 is the residual resistivity, and r is a material-dependent constant which depends on the plasma frequency and electron-phonon coupling strength. The fit using this model in the temperature range 20 K to 300 K yields $\rho_0 = 391(7)$ $\mu\Omega$ cm, $\theta_D = 100(6)$ K, and $r = 53.5(8)$ $\mu\Omega$ cm.

C. Magnetization

The bulk nature of superconductivity in NbReSi is confirmed by dc magnetization measurement in an applied field of 1 mT in ZFCW-FCC mode. The onset of the superconducting state was observed at 6.29(3) K with a strong type-II nature indicated by flux pinning behavior below transition temperature in FCC measurements [see Fig. 3(a)]. The sample with a rectangular cuboid shape was used for magnetization measurements. After correcting the demagnetization factor, the superconducting fraction was found to be close to 100% at 1.8 K.

The field dependence of the dc magnetization was investigated at different temperatures [see Fig. 3(b)]. The magnetization increase linearly with field up to a certain field value and then deviates from linear dependence followed by the reverse in magnetization upon entering the vortex state. The point of deviation from linear behavior is taken as the value of the lower critical field $H_{c1}(T)$. The temperature variation of H_{c1} is well described by Ginzburg-Landau equation, $H_{c1}(T) = H_{c1}(0)(1\text{-}t^2)$, (t = T/T_c), which gives $H_{c1}(0) = 4.32(6)$ mT [see Fig. 3(c)].

The upper critical field for the sample was estimated using the resistivity and ac susceptibility data collected at different applied fields (see inset of Fig. 4). The 50% of the drop in susceptibility/resistivity is considered as the transition at the corresponding field. The upper critical field estimated from resistivity has shown comparatively higher value. This behavior can be attributed to surface or filamentary effects [36,37]. The temperature dependence of the upper critical field estimated from ac susceptibility, as displayed in Fig. 4, has shown an upward curvature at high field. This feature is reminiscent of a two-gap superconductor. The equations for the temperature dependence of the upper critical field in the dirty limit for two gap superconductors are derived, taking account of both interband and intraband scattering. It was found that the nature of the H_{c2}(t) curve essentially depends on the intraband diffusivity and can vary significantly from the one-band superconductors. A fit to the data using a two-gap model, according to which the H_{c2}(t) can be implicitly written in the parametric equation [38–41]

$$\ln\left(\frac{1}{t}\right) = \left[U(s) + U(\eta s) + \frac{\lambda_0}{w}\right] + \left(\frac{1}{4}\left[U(s) - U(\eta s) - \frac{\lambda_-}{w}\right]^2 + \frac{\lambda_{12}\lambda_{21}}{w^2}\right)^{1/2}$$

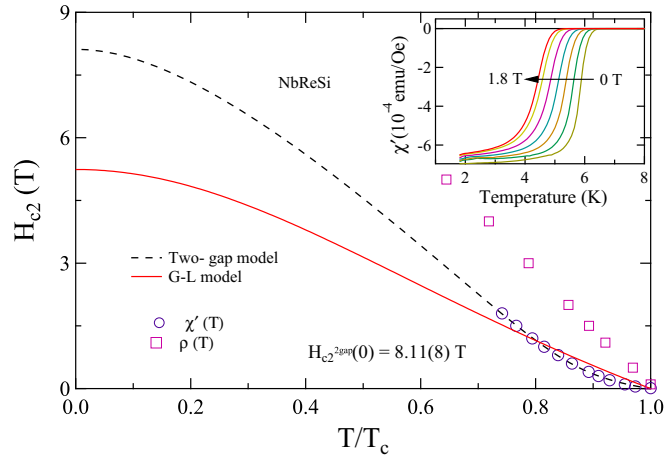

FIG. 4. The temperature dependence of the upper critical field is estimated from ac susceptibility and resistivity measurements. The dotted line shows the fit to the data using the two-gap model, and the solid line shows the GL equation's fit. The estimated $H_{c2}(0)$ is 8.11(8) T. Inset shows the ac susceptibility data taken at different applied fields.

$$H_{c2} = \frac{2\phi_0 T s}{D_1} \quad \eta = \frac{D_2}{D_1}$$
$$U(s) = \psi(s + 1/2) - \psi(1/2). \tag{4}$$

Here, $\lambda_- = \lambda_{11} - \lambda_{22}$, $\lambda_0 = (\lambda_-^2 + 4\lambda_{12}\lambda_{21})$, $w = \lambda_{11}\lambda_{22} - \lambda_{21}\lambda_{12}$. The variables, $\lambda_{11}, \lambda_{22}, \lambda_{12}$, and λ_{21} are the matrix elements of the BCS coupling constants: the diagonal terms λ_{11} and λ_{22} represent the intraband coupling and λ_{12} and λ_{21} represent interband coupling. D_1 and D_1 are the intraband diffusivity at respective bands. ϕ_0 is the flux quantum and $\psi(s)$ is the digamma function. An extrapolation using Eq. (4) to $T = 0$ has yielded $H_{c2}(0) = 8.11(8)$ T. Using the respective values of $H_{c2}(0)$ and $H_{c1}(0)$, the coherence length $\xi_{\rm GL}(0)$ and the magnetic penetration length $\lambda_{\rm GL}(0)$ is calculated as given in Ref. [37] and the values came to be $\xi_{\rm GL}(0) = 64(4)$ Å and $\lambda_{\rm GL}(0) = 3969(64)$ Å while the GL model failed to trace the data points underestimating the $H_{c2}(0)$ value. This value of $H_{c2}(0)$ is greater than those reported for similarly structured materials TaXSi (X = Re/Ru) [37]. Nevertheless, a similar upward curvature in H_{c2}(t) is expected for superconductors if nonmagnetic impurities or disorders are present [38]. A high residual resistivity value and low value of residual resistivity ratio may point toward disorder in this system. To elucidate the gap structure, measurements on high-quality single crystals is required in future.

D. Muon spin rotation and relaxation measurements

We have investigated the system using μSR spectroscopy to get microscopic insight into the superconducting ground state. TF-μSR data was employed to investigate the superconducting gap structure of NbReSi. The magnetic field was applied orthogonal to the initial muon spin direction during this measurement. The sample cooled in an applied field of 40 mT, well above the lower critical field to form a well-ordered flux line lattice (FLL). The inhomogeneous field distribution can account for the rapid depolarization in spectra below the transition temperature due to FLL (Fig. 5).

The spectra can be well described by combining sinusoidally oscillating function damped with Gaussian relaxation and an oscillatory background term:

$$G_{\rm TF}(t) = A_0 \exp\left(\frac{-\sigma^2 t^2}{2}\right)\cos(\omega_1 t + \phi) + A_1 \cos(\omega_2 t + \phi). \tag{5}$$

Here the first term corresponds to the signal from sample, while the second corresponding to signal from the silver sample holder. A_0 and A_1 denote the sample and background asymmetries, while ω_1 and ω_2 correspond to the muon precession frequencies in the sample and background, respectively. The depolarization rate σ in Eq. (5) is comprised of two components, σ_N and $\sigma_{\rm sc}$. σ_N is accounted by the nuclear dipolar moments while $\sigma_{\rm sc}$ accounts for the depolarization rate from the FLL. They are related by $\sigma^2 = \sigma_{\rm sc}^2 + \sigma_{\rm N}^2$. The value of the temperature-independent depolarization from the nuclear moment came to be $\sigma_N = 0.255\ \mu s^{-1}$. Such a not-too-small value for σ_N is observed for several Re-based materials due to the large nuclear magnetic moment of the Re atom [23].

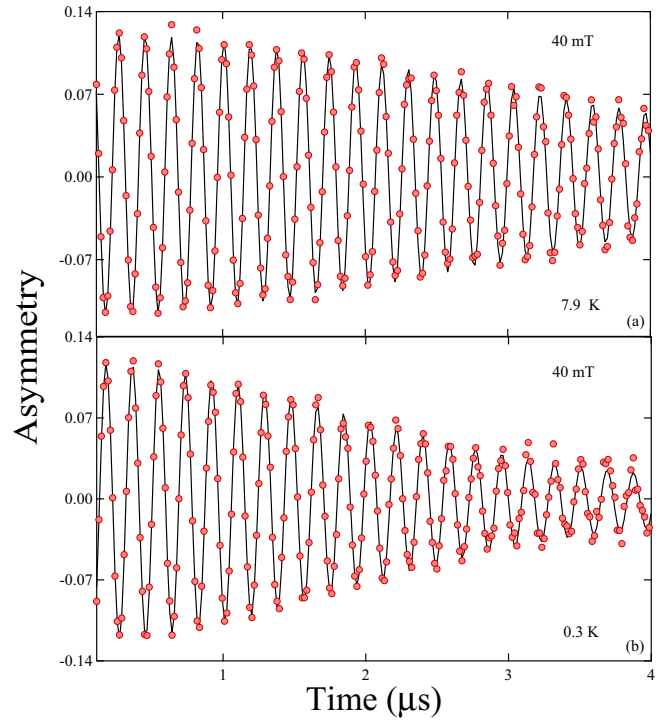

FIG. 5. Transverse field μSR spectra collected at 40 mT at (a) 7.9 K and (b) 0.3 K. The increased depolarization of the muons in the sample due to the flux line lattice formation can be seen in (b).

The temperature dependence of $\sigma_{\rm sc}$ extracted using the above expression is plotted in Fig. 6. The depolarization has showed a plateau at low temperature after which it decreased upon increasing temperature and reaches zero at T_c. This nature can be well followed by the s-wave model in the dirty limit as given by

$$\frac{\sigma_{\rm sc}(T)}{\sigma_{\rm sc}(0)} = \frac{\lambda^{-2}(T)}{\lambda^{-2}(0)} = \frac{\Delta(T)}{\Delta(0)}\tanh\left[\frac{\Delta(T)}{2k_BT}\right], \tag{6}$$

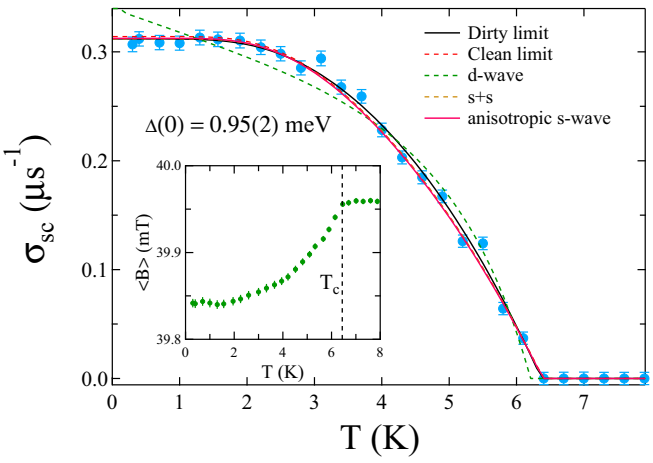

FIG. 6. Muon depolarization rate, $\sigma_{\rm sc}$ collected at 40 mT. The data collected at range of temperature across T_c is well traced by s-wave model giving the superconducting gap as Δ (0) = 0.95(2) meV. The inset shows the temperature dependence of the internal magnetic field.

where $\Delta(T)/\Delta(0) = \tanh\{1.82(1.018(T_c/T-1))^{0.51}\}$ is the BCS approximation for the temperature dependence of the energy gap and $\Delta(0)$ is the gap magnitude at zero temperature, while in the clean limit,

$$\frac{\sigma_{sc}(T)}{\sigma_{sc}(0)} = \frac{\lambda^{-2}(T)}{\lambda^{-2}(0)} = 1 + 2\int_{\Delta(T)}^{\infty}\left(\frac{\delta f}{\delta E}\right)\frac{EdE}{\sqrt{E^2-\Delta^2(T)}}. \tag{7}$$

Here $f = [1+\exp(E/k_BT)]^{-1}$ is the Fermi function and $\Delta(T) = \Delta(0)\tanh\{1.82(1.018(T_c/T-1))^{0.51}\}\, g(\phi)$. The term, $g(\phi)$ accounts for the angular dependence of the gap function, where ϕ is the azimuthal angle. $g(\phi)$ can be substituted with (i) 1 for the s-wave model, (ii) $|\cos(2\phi)|$ for the d-wave model, and (iii) $(1+a\cos(4\phi))/(1+a)$ for anisotropic gap, where a represents the anisotropic parameter [42]. Among the different fitting models employed, the data was best described by dirty limit s-wave model ($\chi^2_{\text{norm.dirty}} = 1.42$ and $\chi^2_{\text{norm.clean}} = 1.77$). The low value of residual resistivity ratio also justifies the dirty limit nature of the sample. The dirty limit s-wave model fitting exactly retraces the path, giving the superconducting gap as $\Delta(0) = 0.95(2)$ meV. This gives the normalized superconducting gap as $\Delta(0)/k_BT_c = 1.73(2)$, showing the moderately coupled nature of the sample, while, in the anisotropic model, the anisotropic parameter, a, has converged to a very small value 0.008(3), which rules out any anisotropic nature of the gap. In the d-wave model, $\chi^2 = 7.4$, negates any d-wave nature. To check any multigap nature as pointed out by susceptibility measurements, we have also performed a two-gap model fitting, where the total depolarization is expressed a sum of two components:

$$\frac{\sigma_{sc}(T)}{\sigma_{sc}(0)} = \omega\frac{\sigma_{sc}(T,\Delta(0)_1)}{\sigma_{sc}(0,\Delta(0)_1)} + (1-\omega)\frac{\sigma_{sc}(T,\Delta(0)_2)}{\sigma_{sc}(0,\Delta(0)_2)}. \tag{8}$$

Here, $\Delta(0)_1$ and $\Delta(0)_2$ are the zero-temperature values of the two gaps. This model gives $\omega = 1$, which converges into a single band model. Hence, in conclusion, the TF-μSR data shows the isotropic s-wave nature of NbReSi. However, it is to be noted that the measurement is performed at an applied field of 40 mT, which could suppress a two-gap nature. Besides this, the dirty limit nature of the samples can also curtail the effects of non-s-wave gap structures. Hence further detailed measurements on high-quality single crystal samples are necessary at low applied fields to unveil the gap structure in this system.

Muons being very sensitive to small magnetic fields can be employed to investigate the system further. A measurement performed in the zero-field and longitudinal geometry (ZF-μSR) can detect a spontaneous magnetic field, if present, below T_c. ZF-μSR spectra collected at two temperatures above and below T_c is shown in Fig. 7. Absence of any precessional signal rules out the presence of any coherent long-range magnetic ordering. In the absence of any atomic moments, the muon depolarization is solely due to randomly oriented nuclear moments, which can be best described by the standard Kubo-Toyabe function given by [43]

$$G_{KT}(t) = \frac{1}{3} + \frac{2}{3}(1-\sigma_{ZF}^2t^2)\exp\left(\frac{-\sigma_{ZF}^2t^2}{2}\right). \tag{9}$$

σ_{ZF} accounts for the relaxation due to static, randomly oriented local fields associated with nuclear moments at the muon site. The obtained relaxation spectra for NbReSi is best described by the function

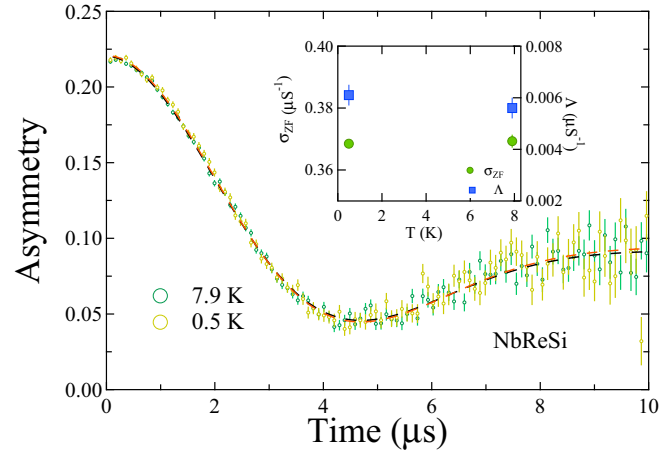

FIG. 7. Longitudinal asymmetry spectra collected at zero field at two different temperatures above and below T_c. Both spectra were seen following the same path, indicating the absence of spontaneous field in the superconducting phase. The dotted lines are the fit to the data using Eq. (10). The inset shows the fitting parameters for the sample.

$$G(t) = A_1\exp(-\Lambda t)G_{KT}(t) + A_{BG}, \tag{10}$$

where A_1, A_{BG} represent the sample and background asymmetry, respectively, while Λ accounts for any additional relaxation rate. Using Eq. (10), an identical relaxation behavior is shown by the spectra collected at temperatures above and below the T_c. The difference in fitting parameters came to be $\Delta\sigma = 0.0008\ \mu s^{-1}$ and $\Delta\Lambda = 0.0005\ \mu s^{-1}$. This small parameter difference indicates the absence of any spontaneous field originating in the superconducting state, showing that the TRS preserved for the NbReSi in the superconducting ground state. At this point, it is worth mentioning that several superconductors have shown spontaneous field and hence the broken TRS despite being in the dirty limit regime [19–24], designating the preserved TRS as the intrinsic nature of NbReSi. The superconducting and normal state properties of NbReSi are summarized in Table I.

TABLE I. Superconducting and normal state parameters for NbReSi.

Parameters	unit	Value
T_c	K	6.29(3)
$H_{c1}(0)$	mT	4.32(6)
$H_{c2}(0)$	T	8.11(8)
$H^p_{c2}(0)$	T	11.51(7)
$\lambda_{GL}(0)$	Å	3969(64)
$\xi_{GL}(0)$	Å	64(4)
θ_D	K	100(6)
$\Delta(0)$	meV	0.95(2)
$\Delta(0)/k_BT_c$		1.73(2)

IV. CONCLUSION

We have characterized the ternary noncentrosymmetric compound NbReSi by x-ray diffraction, magnetization, resistivity, and muon spectroscopy measurements. The results indicate NbReSi enters the superconducting state below $T_c = 6.29$ K and show a strong type-II behavior. The upper critical field curve estimated from ac susceptibility data has shown an upward curvature, reminiscent of two-gap superconductivity. However, this nature can also arise due to disorder in the system. The transverse field μSR measurements confirmed a moderately coupled, BCS-type isotropic superconducting gap with $\Delta(0)/k_BT_c = 1.73$, indicating disorder/inhomogeneity may give rise to the upward curvature of H_{c2}. Further detailed measurements on single crystal samples are required to state the gap structure in NbReSi conclusively. The zero field measurements showed TRS preserved in the superconducting ground state. This result asks for further studies in Re-based compounds to understand the sceptical role of elemental Re in many unconventional superconducting systems.

Note added. Recently, we became aware that superconductivity was reported on the same compound by Su *et al.* [44].

ACKNOWLEDGMENTS

R.P.S. acknowledges Science and Engineering Research Board, Government of India, for the Core Research Grant No. CRG/2019/001028. We thank Newton Bhabha for funding and ISIS, STFC, UK, for the muon beam time to conduct the μSR experiments.

[1] E. Bauer and M. Sigrist, *Non-centrosymmetric Superconductor: Introduction and Overview* (Springer-Verlag, Heidelberg, 2012).
[2] M. Smidman, M. B. Salamon, H. Q. Yuan, and D. F. Agterberg, Rep. Prog. Phys. **80**, 036501 (2017).
[3] E. Bauer, G. Hilscher, H. Michor, Ch. Paul, E. W. Scheidt, A. Gribanov, Yu. Seropegin, H. Noël, M. Sigrist, and P. Rogl, Phys. Rev. Lett. **92**, 027003 (2004).
[4] A. P. Schnyder and S. Ryu, Phys. Rev. B **84**, 060504(R) (2011).
[5] A. P. Schnyder, P. M. R. Brydon, and C. Timm, Phys. Rev. B **85**, 024522 (2012).
[6] L. P. Gor'kov and E. I. Rashba, Phys. Rev. Lett. **87**, 037004 (2001).
[7] P. A. Frigeri, D. F. Agterberg, A. Koga, and M. Sigrist, Phys. Rev. Lett. **92**, 097001 (2004).
[8] P. A. Frigeri, D. F. Agterberg, and M. Sigrist, New J. Phys. **6**, 115 (2004).
[9] I. Bonalde, W. Bramer-Escamilla, and E. Bauer, Phys. Rev. Lett. **94**, 207002 (2005).
[10] H. Mukuda, T. Fujii, T. Ohara, A. Harada, M. Yashima, Y. Kitaoka, Y. Okuda, R. Settai, and Y. Onuki, Phys. Rev. Lett. **100**, 107003 (2008).
[11] S. Kuroiwa, Y. Saura, J. Akimitsu, M. Hiraishi, M. Miyazaki, K. H. Satoh, S. Takeshita, and R. Kadono, Phys. Rev. Lett. **100**, 097002 (2008).
[12] A. D. Hillier, J. Quintanilla, and R. Cywinski, Phys. Rev. Lett. **102**, 117007 (2009).
[13] V. M. Edelstein, Phys. Rev. Lett. **75**, 2004 (1995).
[14] S. Fujimoto, Phys. Rev. B **72**, 024515 (2005).
[15] M. Z. Hasan and C. L. Kane, Rev. Mod. Phys. **82**, 3045 (2010).
[16] X.-L. Qi and S.-C. Zhang, Rev. Mod. Phys. **83**, 1057 (2011).
[17] M. Sato and S. Fujimoto, Phys. Rev. Lett. **105**, 217001 (2010).
[18] M. Z. Hasan and J. E. Moore, Annu. Rev. Condens. Matter Phys. **2**, 55 (2011).
[19] J. A. T. Barker, D. Singh, A. Thamizhavel, A. D. Hillier, M. R. Lees, G. Balakrishnan, D. McK. Paul, and R. P. Singh, Phys. Rev. Lett. **115**, 267001 (2015).
[20] D. Singh, M. S. Scheurer, A. D. Hillier, D. T. Adroja, and R. P. Singh, Phys. Rev. B **102**, 134511 (2020).
[21] Arushi, D. Singh, A. D. Hillier, M. S. Scheurer, and R. P. Singh, Phys. Rev. B **103**, 174502 (2021).
[22] R. P. Singh, A. D. Hillier, B. Mazidian, J. Quintanilla, J. F. Annett, D. M. Paul, G. Balakrishnan, and M. R. Lees, Phys. Rev. Lett. **112**, 107002 (2014).
[23] D. Singh, J. A. T. Barker, A. Thamizhavel, D. McK. Paul, A. D. Hillier, and R. P. Singh, Phys. Rev. B **96**, 180501(R) (2017).
[24] D. Singh, K. P. Sajilesh, J. A. T. Barker, D. McK. Paul, A. D. Hillier, and R. P. Singh, Phys. Rev. B **97**, 100505(R) (2018).
[25] T. Shang, M. Smidman, A. Wang, L.-J. Chang, C. Baines, M. K. Lee, Z. Y. Nie, G. M. Pang, W. Xie, W. B. Jiang, M. Shi, M. Medarde, T. Shiroka, and H. Q. Yuan, Phys. Rev. Lett. **124**, 207001 (2020).
[26] T. Shang, M. Smidman, S. K. Ghosh, C. Baines, L. J. Chang, D. J. Gawryluk, J. A. T. Barker, R. P. Singh, D. McK. Paul, G. Balakrishnan, E. Pomjakushina, M. Shi, M. Medarde, A. D. Hillier, H. Q. Yuan, J. Quintanilla, J. Mesot, and T. Shiroka, Phys. Rev. Lett. **121**, 257002 (2018).
[27] T. Shang, C. Baines, L. J. Chang, D. J. Gawryluk, E. Pomjakushina, M. Shi, M. Medarde, and T. Shiroka, npj Quantum Mater. **5**, 76 (2020).
[28] P. K. Biswas, M. R. Lees, A. D. Hillier, R. I. Smith, W. G. Marshall, and D. M. Paul, Phys. Rev. B **84**, 184529 (2011).
[29] J. A. T. Barker, B. D. Breen, R. Hanson, A. D. Hillier, M. R. Lees, G. Balakrishnan, D. McK. Paul, and R. P. Singh, Phys. Rev. B **98**, 104506 (2018).
[30] T. Shang, A. Amon, D. Kasinathan, W. Xi, M. Bobnar, Y. Chen, A. Wang, M. Shi, M. Medarde, H. Q. Yuan, and T. Shiroka, New J. Phys. **21**, 073034 (2019).
[31] G V Subba Rao, K. Wagner, G. Balakrishnan, J. Janaki, W. Paulus, R. Schollhorn, V. S. Subramanian, and U. Poppe, Bull. Mater. Sci. **7**, 215 (1985).
[32] S. Bağcı, M. Cin, H. Y. Uzunok, E. Karaca, H. M. Tutuncu, and G. P. Srivastava, Phys. Rev. B **100**, 184507 (2019).
[33] A. D. Hillier, J. S. Lord, K. Ishida, and C. Rogers, Philos. Trans. R. Soc. A **377**, 20180064 (2019).
[34] T. Roisnel and J. Rodriguez-Carvajal, Mater. Sci. Forum **378**, 118 (2001).

[35] G. Grimvall, *The Electron-Phonon Interaction in Metals* (North Holland, Amsterdam, 1981).
[36] F. Kneidinger, H. Michor, A. Sidorenko, and E. Bauer, I. Zeiringer and P. Rogl, C. Blaas-Schenner, D. Reith, and R. Podloucky, Phys. Rev. B **88**, 104508 (2013).
[37] K. P. Sajilesh and R. P. Singh, Supercond. Sci. Technol. **34**, 055003 (2021).
[38] A. Gurevich, Phys. Rev. B **67**, 184515 (2003).
[39] Y. Li, W. Tabis, Y. Tang, G. Yu, J. Jaroszynski, N. Barisic, and M. Greven, Sci. Adv. **5**, eaap7349 (2019).
[40] F. Hunte, J. Jaroszynski, A. Gurevich, D. C. Larbalestier, R. Jin, A. S. Sefat, M. A. McGuire, B. C. Sales, D. K. Christen, and D. Mandrus, Nature (London) **453**, 903 (2008).
[41] C. Q. Xu, B. Li, J. J. Feng, W. H. Jiao, Y. K. Li, S. W. Liu, Y. X. Zhou, R. Sankar, N. D. Zhigadlo, H. B. Wang, Z. D. Han, B. Qian, W. Ye, W. Zhou, T. Shiroka, P. K. Biswas, X. Xu, and Z. X. Shi, Phys. Rev. B **100**, 134503 (2019).
[42] R. Khasanov, K. Conder, E. Pomjakushina, A. Amato, C. Baines, Z. Bukowski, J. Karpinski, S. Katrych, H. H. Klauss, H. Luetkens, A. Shengelaya, and N. D. Zhigadlo, Phys. Rev. B **78**, 220510(R) (2008).
[43] R. S. Hayano, Y. J. Uemura, J. Imazato, N. Nishida, T. Yamazaki, and R. Kubo, Phys. Rev. B **20**, 850 (1979).
[44] H. Su, T. Shang, F. Du, C. F. Chen, H. Q. Ye, X. Lu, C. Cao, M. Smidman, and H. Q. Yuan, Phys. Rev. Materials **5**, 114802 (2021).